AD-A158 594 THE DETECTION OF FAINT SPACE OBJECT WITH SOLID STATE IMAGE DETECTORS(U) MICHIGAN UNIV ANN ARBOR DEPT OF PHYSICS D J HEGYI 19 MAR 85 AFOSR-TR-85-0389 1/1

UNCLASSIFIED AFOSR-80-0095 F/G 3/1 NL

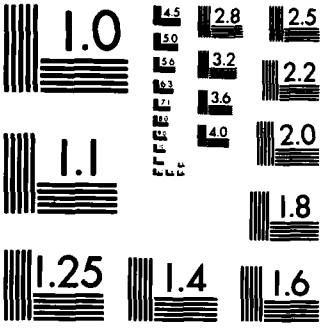

Final Technical Report

Submitted to

U.S. Air Force Office of Scientific Research

Grant AFOSR-80-0095
"The Detection of Faint Space Object with Solid State Imaging Detectors"

Grant Period: January 1, 1980 - January 31, 1985

Total Amount Awarded: $500,828

Principal Investigator: Dennis J. Hegyi
Associate Professor of Physics
University of Michigan
Ann Arbor, MI 48109-1120

March 19, 1985

UNCLASSIFIED
SECURITY CLASSIFICATION OF THIS PAGE

AD-A158594

REPORT DOCUMENTATION PAGE

1a. REPORT SECURITY CLASSIFICATION: Unclassified	1b. RESTRICTIVE MARKINGS
2a. SECURITY CLASSIFICATION AUTHORITY	3. DISTRIBUTION/AVAILABILITY OF REPORT: Approved for public release; Distribution unlimited
2b. DECLASSIFICATION/DOWNGRADING SCHEDULE	
4. PERFORMING ORGANIZATION REPORT NUMBER(S)	5. MONITORING ORGANIZATION REPORT NUMBER(S): AFOSR-TR- 85-0389
6a. NAME OF PERFORMING ORGANIZATION: University of Michigan; 6b. OFFICE SYMBOL (If applicable):	7a. NAME OF MONITORING ORGANIZATION: AFOSR
6c. ADDRESS (City, State and ZIP Code): Department of Physics, Ann Arbor, MI 48109-1120	7b. ADDRESS (City, State and ZIP Code): Building 410, Bolling AFB DC 20332-6448
8a. NAME OF FUNDING/SPONSORING ORGANIZATION: AFOSR; 8b. OFFICE SYMBOL (If applicable): NP	9. PROCUREMENT INSTRUMENT IDENTIFICATION NUMBER: AFOSR 80-0095
8c. ADDRESS (City, State and ZIP Code): Building 410, Bolling AFB DC 20332-6448	10. SOURCE OF FUNDING NOS.

PROGRAM ELEMENT NO.	PROJECT NO.	TASK NO.	WORK UNIT NO.
61102F	2311	A1	

11. TITLE (Include Security Classification): "THE DETECTION OF FAINT SPACE OBJECTS WITH SOLID STATE IMAGING DETECTORS"

12. PERSONAL AUTHOR(S): Dr Dennis J. Hegyi

13a. TYPE OF REPORT	13b. TIME COVERED	14. DATE OF REPORT (Yr., Mo., Day)	15. PAGE COUNT
FINAL	FROM 01 Jan 80 TO 31 Jan 85	19 Mar 85	15

16. SUPPLEMENTARY NOTATION

17. COSATI CODES			18. SUBJECT TERMS (Continue on reverse if necessary and identify by block number)
FIELD	GROUP	SUB. GR.	

19. ABSTRACT (Continue on reverse if necessary and identify by block number)

The primary focus of research during this funding period has been to obtain information with the highest signal-to-noise ratio from faint astronomical sources using a charge-coupled device (CCD). The starting point of the investigation was to determine the optimal sampling function for CCDs considering the noise spectrum characteristic of real devices; the noise spectrum of most CCDs can be accurately described by a combination of 1/f and white noise. Then, a CCD system was constructed so that all operating parameters could be easily adjusted. Some unexpected improvements in performance were obtained by optimizing the operating temperature and increasing the number of electrode voltages which could be independently set compared to other CCD systems. The next phase of the investigation was to develop an image processing system to extract, in a statistically correct way, as much information as possible from astronomical images. The system was then applied to problems ranging from speckle interferometry to global cosmolical tests including an ivestigation to determine the nature of the dark matter in the halos of spiral galaxies.

20. DISTRIBUTION/AVAILABILITY OF ABSTRACT	21. ABSTRACT SECURITY CLASSIFICATION
UNCLASSIFIED/UNLIMITED ☒ SAME AS RPT. ☐ DTIC USERS ☐	Unclassified

22a. NAME OF RESPONSIBLE INDIVIDUAL	22b. TELEPHONE NUMBER (Include Area Code)	22c. OFFICE SYMBOL
Dr Henry R. Radoski	202/767-4906	NP

DD FORM 1473, 83 APR — EDITION OF 1 JAN 73 IS OBSOLETE.

UNCLASSIFIED
SECURITY CLASSIFICATION OF THIS PAGE

SUMMARY

The primary focus of research during this funding period has been to obtain information with the highest signal-to-noise ratio from faint astronomical sources using a charge-coupled device (CCD). The starting point of the investigation was to determine the optimal sampling function for CCDs considering the noise spectrum characteristic of real devices; the noise spectrum of most CCDs can be accurately described by a combination of 1/f and white noise. Then, a CCD system was constructed so that all operating parameters could be easily adjusted. Some unexpected improvements in performance were obtained by optimizing the operating temperature and increasing the number of electrode voltages which could be independently set compared to other CCD systems. The next phase of the investigation was to develop an image processing system to extract, in a statistically correct way, as much information as possible from astronomical images. The system was then applied to problems ranging from speckle interferometry to global cosmological tests including an investigation to determine the nature of the dark matter in the halos of spiral galaxies.

The Final Report

Research during the funding period of this grant can be divided into three main areas: the development of a charge-coupled device (CCD) imaging system, the development of software to analyze CCD astronomical images, and the scientific progress obtained both with and without the CCD. We shall begin by providing a brief introduction to CCDs. The emphasis in our discussion will be to provide information which might be of interest to anyone building a CCD system and which may not be generally known.

A CCD is a mosaic of photodetectors fabricated on a silicon substrate. CCDs represent an enormous step forward in imaging detectors in that they have properties which are close to that of an ideal detector. CCDs have quantum efficiencies of 50 per cent, are linear over dynamic ranges of 10,000 and have stabilities of better than one part in 1000. While imaging systems based on CCDs appear to have enormous potential, it has been very difficult to build working systems which exploit the device's potential. The electronics to operate CCDs are complex and there are many operating parameters which must be carefully adjusted for the device to function, much less to function well.

One of our primary accomplishments has been to work out several basic issues related to CCD signal extraction. We have calculated the optimal sampling function for CCDs so that information can be extracted as effectively as possible. Also, we have determined the signal-to-noise ratio for the optimal sampling function so that it is possible to compare several popular sampling functions with the optimal to know what improvements might be possible. These results have been derived for CCDs which exhibit a combination of 1/f and white noise. Such noise spectra closely model the noise in real CCDs.

Using these theoretical results as a guide we built a very flexible CCD system so that virtually all CCD parameters could be easily and conveniently adjusted to optimize the response of the system. To accomplish this, all 29 timing parameters can be changed from a computer keyboard in increments of 100 ns.

In addition, we found it was important to keep the electronics as flexible as possible. Our system, designed for a thinned RCA CCD, was built with 17 adjustable power supplies. There is some advantage in using this number of supplies over, for example, 11, but the advantage is not large. Using less than 11 supplies, however, would result in degraded performance. Specifically, we found that it was very important to have separate high and low voltage controls for each of the three horizontal clocks. Also, we found that the CCD performance was improved by using three different voltage levels for the vertical clocks. On the other hand, we found that separate supplies for each of the three vertical clocks were not particularly important. Other supplies are for phase reset and for RD.

During the process of optimizing the performance of the CCD we were surprised to find that the resolution of the CCD depended sensitively on the operating temperature of the device. There was an optimal temperature with a characteristic width of about 10 degrees Centigrade. We have no way of knowing whether this temperature dependence is characteristic of CCDs in general or is only characteristic of our CCD, but it does seem to be reasonably consistent with the physics of CCDs.

As we shall discuss below, the 1/f noise in the output on-chip FET amplifier is responsible for the readout noise. Because noise in any of the supply voltages couples to the on-chip amplifier, it is important to minimize power supply noise. We constructed power supplies using standard single chip IC regulators. These devices have good noise specifications at high frequencies but not at the low frequencies at which we sample our CCDs. To remedy this, we used toroidally wound inductors in series with the power input to the regulator chips. The equivalent noise of our electronics is 5 electrons, which, because it adds in quadrature to the readout noise, only increases the readout noise by a negligible amount.

To test that we understand the origin of the readout noise, we have calculated the readout noise using the measured CCD capacitance, the measured 1/f noise of the on-chip amplifier, and our sampling function. The calculated noise is 57 electrons with an estimated error of 6 electrons, and the measured readout noise is 64 electrons, in reasonable agreement.

The CCD system is managed by a NOVA minicomputer which we use to download the CCD control microprocessor and to analyze images at the telescope. The NOVA is programmed in FORTH and has a variety of routines to perform simple picture processing at the telescope. A particularly convenient routine that we have written for focussing the telescope when the CCD is in operation displays a cross-section of the stellar image on the TV monitor and also displays the calculated full-width-half-maximum in pixels. Since the display is updated every second it greatly simplifies focussing.

Image processing at Michigan is carried out on a VAX/780 computer. Attached to the computer is a Grinnell GMR270 which is capable of displaying images on a color TV monitor in 4096 pseudocolors.

The image processing system that we use started out as a set of basic image processing programs written at Mt. Stromlo Observatory. We have added to the programs so that we can analyze data from any two-dimensional detector

and produce outputs on a variety of output devices. Programs are now available to perform arithmetic functions on images, to carry out photometry on both stars and galaxies, to flat-field CCD images, and to analyze speckle interferometry images.

Stellar photometry can be easily carried out on stars covering a wide range of intensities. The brightest stars, which have the highest photometric accuracy, cannot be used for calibration on most CCD systems because for typical exposure times they saturate the system. We use bright stars for calibration by using short shutter speeds and by defocussing the stellar image. This technique allows us to obtain photometric calibrations to better than one per cent on the best bright reference stars.

Considerable effort has gone into writing software for the reduction of two-dimensional surface photometry of elliptical galaxies. We now have routines which can do a weighted least-squares fit of any chosen surface-brightness formula to the surface brightness distribution of an elliptical galaxy while taking into account overlapping stars and galaxies, including "seeing effects" due to the earth's atmosphere, yielding the fitting parameters of the formula with the associated errors. Some of our surface brightness measurements reach to beyond 30th magnitude, fainter than any previously published results.

One interesting application of our elliptical galaxy fitting routine was to fit a bright elliptical galaxy that was partially overlapping the images of other faint ellipticals and to completely subtract out the image of the bright galaxy. This method could also be used to obtain images of individual objects in a cluttered field. Elliptical contours are a fair approximation to the isophotes of a symetrical object.

A group of programs has been written to reduce speckle interferometric data. This data is obtained from a 64x64 area of pixels closest to the readout amplifier to minimize charge smearing by minimizing the number of charge transfers to the readout amplifier and to perform the readout as quickly as possible. The power spectrum of several hundred images of a binary star is divided by the power spectrum of a corresponding number of images of a nearby calibration star. From the ratio of power spectra it is possible to obtain the angular separation, position angle, and relative intensity of an otherwise unresolvable binary system. The advantage of our system over other speckle interferometric systems is that we use no image intensifier, which, though it limits us to stars brighter than 10th magnitude on a 52 inch telescope, takes advantage of the high intrinsic stability of the CCD.

We shall now discuss scientific research accomplishments during the period of the grant. Below, we shall discuss scientific progress in four different research areas: global cosmological tests, the resolution of the binary star system Mu-Cassiopeiae and a measurement of the primordial helium abundance, and cosmological dark matter.

Global cosmological tests are the best way to determine the future expansion of the universe -- Will it expand forever or will it eventually collapse and fall back on itself? At the present time it appears possible to use CCDs to determine the answer to this question. We have been working on two

cosmological tests, the metric angular diameter and the redshift-magnitude tests. It appears to be possible to carry out both tests using the same set of data. The problems at the present time center on being able to reduce systematic errors in the collected data so that they do not bias the results. At the present time, our work looks promising and we believe that we shall be able to separate the two most troublesome systematics, mergers of galaxies and stellar luminosity evolution.

We are in the process of writing up a study on the distant cluster of galaxies, Abell 1689. We have collected photometric data in two colors on over 200 elliptical galaxies in the cluster. This rich cluster of galaxies consists of many overlapping images and has never been adequately analyzed. Also, many of the galactic images are quite small and have been smeared out significantly by atmospheric turbulence so that it is necessary to correct for such effects. We accomplish this by using the images of stars in the CCD frame that surround the galaxy of interest.

By making a plot for the cluster of the characteristic size versus magnitude of the galaxies, it has been possible to find a range of galaxies that show no dynamical evolution. Because only the brightest galaxies show effects of mergers and only the faintest galaxies show effects of tidal distortion, there is a middle range of galaxies that reveal none of these dynamical problems. However, these galaxies are affected by stellar evolution. But, if only stellar evolution is present, it is possible to deduce the amount of it because the surface brightest of galaxies should scale as the fourth power of the redshift. Any deviation from it indicates stellar evolution, the amount of which can then be deduced. Perhaps the most interesting aspect of this work from the point of view of other applications is that it is an example of treating data consisting of small, faint images which must be corrected for atmospheric smearing in a statistically correct manner to extract as much information as possible.

We have been making progress towards the resolution of the components of the binary star system Mu-Cassiopeiae. The two stars are separated by about an arc second and differ by a factor of several hundred in intensity in the visible. It is the close separation and the large difference in intensity between the two stars which has made the problem so difficult. With one accurate measurement of the separation between the components it is possible to determine the mass of the stars and then, with other information already available, it is possible to use the theory of stellar interiors to determine the helium abundance of the stars. Data has been obtained on Mu-Cas during several different runs. On each run some new information was obtained so that the observing technique and the method of analysis gradually improved to the extent that this past January we were able to obtain some very high quality data which has yielded an accurate measurement of the separation between the stars. One of the key points that we needed to learn is that it is necessary to choose a calibration star as close on the sky to Mu-Cas as possible and to also observe it as close in time as possible. By limiting the spectral passband of the instrument to about 1000 Angstroms we found that it was not necessary to choose a star that matched the spectral characteristics of Mu-Cas.

A long term project on which we have been working has been to study the nature of the dark matter in the halo of spiral galaxies. Evidence to support

the existence of dark matter in halos is quite compelling. The rotation curves of spiral galaxies must satisfy the equilibrium condition that the centripetal acceleration necessary for circular motion be due to the gravitational acceleration of the matter in the galaxy. However, the matter contained in the visible stars in galaxies is not sufficient to explain the observed gravitational acceleration. The conclusion is that there must be large amounts of unseen mass. The problem on which we have been working is to try to understand the nature of this dark matter.

One part of the study has been to obtain the best limits on the surface brightness of the halo of the edge on spiral galaxy NGC 4565 because it has a well determined rotation curve. Then, with measurements of the surface brightness of the halo, it is possible to calculate the mass-to-light ratio of the dark matter in the halo. We have previously made observations with an instrument designed to search for low surface brightness objects. But, we have also used our CCD system to obtain a better limit on the surface brightness of the halo of NGC 4565. This is actually a difficult observing problem for CCDs because the halo is considerably larger than the field of view of the CCD and so close to the galaxy it is not possible to observe the halo and the background sky in the same exposure. Instead, it was necessary to take three exposures, stepping out from the center of the galaxy with overlap between the exposures. With this technique it has been posible to reach surface brightnesses at the level of a few ten-thousandths of the sky. By fitting the observed surface to the expected 1/r form for the projected distribution of the dark matter, it is possible to determine an upper limit on the mass-to-light ratio of the dark halo matter.

K. Olive (Fermilab) and D. Hegyi have used this data to present a series of arguments concluding that it is quite unlikely that the dark halos can be composed of baryonic matter. Specifically, a halo of gas, dust and rocks, snowballs, low mass stars, planets, dead stars or neutron stars is shown to be unlikely. We briefly summarize the arguments. A gaseous halo will quickly collapse and heat up giving off more X-rays than is consistent with upper limits on the X-ray background. A halo composed of dust or rocks would have contaminated the gas that formed stars in the galactic disk with an excessively high metal abundance. Snowballs would have evaporated very quickly. Low mass stars will give off too much light to go undetected in the optical observations discussed above. Planets, since they may be expected to be a continuation of the same mass distribution function that lead to stars, are also excluded when one considers the arguments in detail. Finally, black holes and neutron stars are not allowed because the ejecta of the parent star that leads to either a white dwarf or neutron star would contaminate with too high a metal abundance a latter generation of stars that formed in the disk.

Publications

1. "Optimal Sampling of Charge-Coupled Devices" Hegyi, D.J. and Burrows, A.S. Astronomical Journal 85, 1421 (1980)

2. "Can Massive Halos be Baryonic?" Hegyi, D.J. Proceedings of the Moriond Astrophysics Meeting, March 1983, La Plagne, France, Eds. J. Audouze, and J. Tran Thranh Van, NATO

3. "Can Galactic Halos be Made of Baryons?" Hegyi, D.J. and Olive, K.A. Phys. Letters 126B, 28 (1983)

4. "Are Massive Halos Baryonic?" Olive K.A. and Hegyi, D.J. Proceedings of the Inner Space/Outer Space Meeting, Fermilab, May 1984, Eds. Kolb, E. and Turner, M.

5. "The Design and Construction of a Charge-Coupled Device Imaging System" Gudehus, D.H. and Hegyi, D.J. Astronomical Journal 90, 130 (1985)

6. "A Case Against Baryons in Galactic Halos" Hegyi, D.J. and Olive, K.A. submitted to the Astrophysical Journal

7. "Excluding Black Holes as the Dark Matter in the Galactic Disk" Hegyi, D.J. Kolb, E., and Olive, K.A. in preparation

8. "A Photometric Study of Abell 1689" Gudehus, D.H. and Hegyi, D.J. in preparation

Personnel

Postdoctoral Associate Adam Burrows has worked on this project from January through August, 1980.

Beginning in February, 1981, Assistant Research Scientist Donald Gudehus joined this program and is still part of the group.

Also, graduate students James Haywood, who is working on speckle interferometry, and Jeffrey Youngen, who is working on galactic evolution, have been supported by this grant.

Interactions

During the term of this grant D. Hegyi has presented talks at the following universities: Chicago, Cambridge, Bolognia, Florence, Tel-Aviv, Yale, and Brown. Also, he has presented talks at the following research institutes: Nordita, Institut d'Astrophysique, CERN, and Fermilab.

THE ASTRONOMICAL JOURNAL VOLUME 90, NUMBER 1 JANUARY 1985

THE DESIGN AND CONSTRUCTION OF A CHARGE-COUPLED DEVICE IMAGING SYSTEM

DONALD H. GUDEHUS AND DENNIS J. HEGYI
The Harrison M. Randall Laboratory of Physics, The University of Michigan, Ann Arbor, Michigan 48109

Received 2[illegible] June 1984; revised 5 October 1984

ABSTRACT

The design and construction of a charge-coupled device (CCD) imaging system optimized for the detection of low surface brightness objects is discussed in detail. In particular, we describe the design of the Dewar and the CCD electronics, as well as the choice of CCD operating voltages, clock timings, and operating temperature. In addition, we discuss the measurement of readout and spatial noise for an RCA SID53612 thinned CCD (320 by 512 pixels). For this chip, we find a readout noise of 64 electrons and obtain a well depth in excess of 350 000 electrons with essentially no blemishes or bleeding of charge on bright star images. The threshold level for trailing of charge is 300 electrons in the center of the chip and is essentially zero in the corner of the chip which is read out first. On broadband exposures, fringing from night-sky lines is typically seen only in the infrared (~8700 Å) at about 2% of the night-sky level. Our twilight flat-field exposures taken on different nights are consistent with each other at a level varying from one part in 100 000 to a few parts in 10 000 on the large scale, and the zero level is stable to ± 10 electrons over a night. The system is linear over its entire range, and we can currently do photometry to better than 0.8% using standard stars.

I. INTRODUCTION

The invention of the charge-coupled device (CCD) by Amelio, Tompsett, and Smith (1970), and its subsequent development over the past decade, has provided astrophysicists with an almost ideal photon detector between the wavelengths of 0.35 and 1.0 μ. A CCD is a solid-state device which, when struck by photons, will produce electron-hole pairs with high efficiency. The electrons are stored in a mosaic of electrostatic potential wells formed by a polysilicon electrode structure and ion implants, while the holes are repelled from the wells. In the thick version of the RCA CCD (SID52501), the photons must pass through the polysilicon electrodes which are highly absorbing in the UV, whereas in the thinned CCD (SID53612), the silicon substrate is etched to extreme thinness so that the photons can enter through the backside of the chip, avoiding the absorptive electrode structure. In both CCD's, the entire imaging area is light sensitive; there are no "dead regions" along the edges of pixels. Also, because the thick CCD is many times more sensitive to cosmic rays than the thinned chip, the thinned CCD has been preferred for use as a photodetector by astrophysicists when long integration times are required.

To read out an image stored in the CCD, the electrode structure which helps form the potential wells is used to transfer the charge from the pixels to a charge-sensitive output amplifier located on the chip. In operation, charge is first shifted vertically, one row at a time, to a horizontal register. The charge is then shifted out of the horizontal register one column at a time to the on-chip amplifier consisting of a small capacitor (~0.5 pF) whose voltage is sampled by an on-chip FET source follower. The change in voltage of the capacitor is directly proportional to the amount of charge deposited, and, consequently, is directly proportional to the number of photons incident on a pixel.

The advantages of a CCD are high quantum efficiency (80% peak), spatially digitized output, geometric stability, large dynamic range (5500), and excellent linearity. All existing CCD's, however, suffer from nonzero readout noise ranging from about 10 to 100 electrons and, for very low light levels, a less than perfect charge-transfer efficiency which gives rise to a "threshold effect" which can complicate applications to spectroscopy and astrometry. However, at higher background light levels, the threshold effect is no longer a problem, and at still higher background light levels, the readout noise is dominated by shot noise. Blemishes and fringing (the interference of light between the front and back faces of a CCD) can further complicate the data analysis. From the experiences of various groups who have built CCD imaging systems (Low 1977 and 1981; Dewey and Ricker 1980; Leach, Schild, Gursky, Madejski, Schwartz, and Weekes 1980; Marcus, Nelson, and Lynds 1979; Meyer and Ricker 1980; Robinson 1981; Wright and Mackay 1981), from our own experience, and from inspection of published CCD pcitures, it is clear that the above problems are serious. Accordingly, we shall discuss aspects of the CCD system relevant to these issues in greater detail.

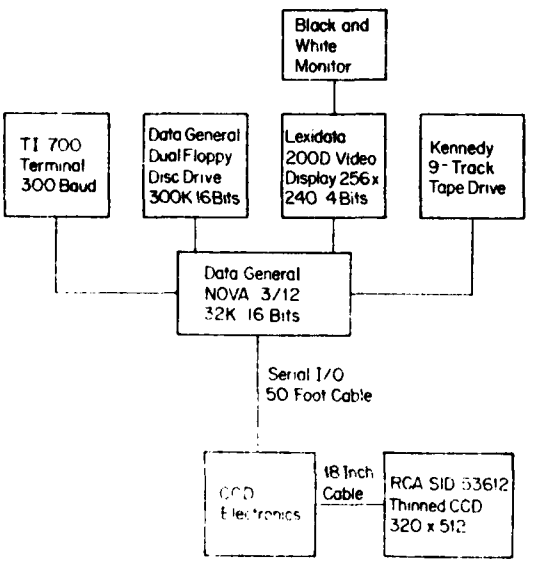

FIG. 1. Block diagram of the CCD operating system.

 0004-6256/85/010130-09$00.90

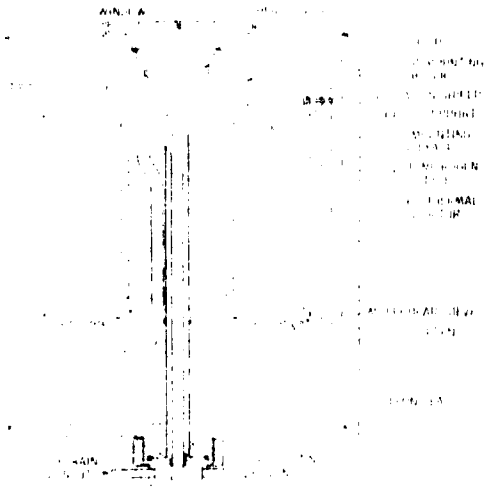

FIG. 2. Schematic diagram of the CCD Dewar.

II. SYSTEM CONTROL

Figure 1 shows an overview of our CCD system. We use a Data General NOVA 3/12 minicomputer to provide the overall control of the CCD system. The selection of a NOVA as a host computer may seem somewhat dated at the present time, but in 1978, when the design and construction was started by one of us (DH), it was a reasonable choice and was available from another project. The NOVA supervises an exposure by loading the memory of the CCD control microprocessor located near the CCD by opening, timing, and closing the shutter, by initiating the readout, and by transferring the data to the magnetic-tape unit for storage. In addition, data can be transferred from tape to floppy disk for processing, to a TV monitor via the Lexidata for display, or to the TTY. All the NOVA programming has been carried out in FORTH which has proven to be very convenient.

We shall now discuss the system in more detail. Communication between the NOVA minicomputer, located in an observing room near the dome, and the CCD electronics, mounted beneath the Dewar on the telescope, is via a serial link over a 50-ft cable. The NOVA transmits (downloads) machine code over the cable in the form of 256 48-bit numbers to the memory of an AM2910 microprocessor which generates the necessary timing signals for control of the CCD. We chose this particular microprocessor because it was the fastest microprocessor available at the time we designed the system. Its cycle time is 100 ns. Additional machine code is used for control of the shutter, for the filter wheel, and to adjust voltages on the CCD.

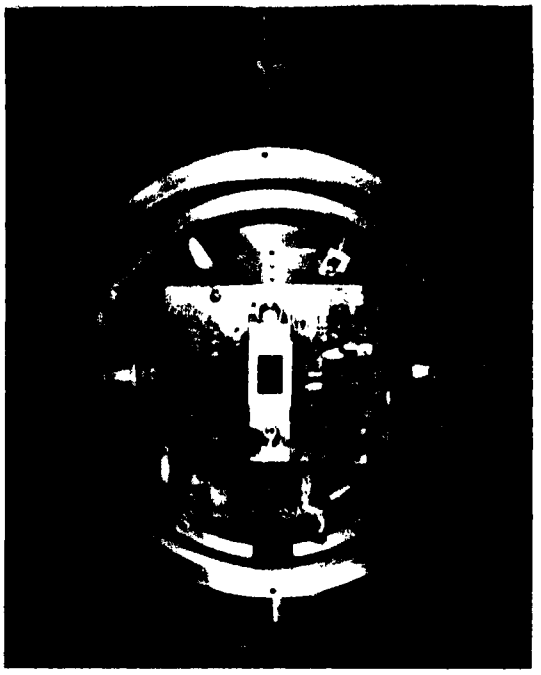

FIG. 3. View of the top of the opened Dewar.

Readout of the CCD, sampling and digitization of the output, and transfer to magnetic tape is accomplished in 50 s by making use of a double buffer programmed into the NOVA's memory. During an exposure, the time remaining in the integration is displayed on the monitor. A maximum of 55 full-frame exposures can be stored on a 1200-ft reel of tape.

Through the TI Silent 700 hard-copy terminal, a user can enter a variety of commands into the system for displaying gray-scale data, graphing data, rapidly reading out a 64×64-pixel region for focusing the telescope, performing speckle interferometry, doing photometry, and performing picture arithmetic. (The hard copy has proven useful for resolving discrepancies in the observing log.)

Under software control, the user may display any four bits of the 14 bits of digitized intensity information from any 256×240-pixel subsection of the CCD frame by loading the data into the Lexidata 200D video generator. The user can also graph horizontal, vertical, or diagonal cuts through the data to further examine a feature. These cuts can be used to calculate the full-width-half-maximum (FWHM) of a feature, which is useful for several modes of operation, but most typically, focusing. In the focusing mode, a repetitive cycle is

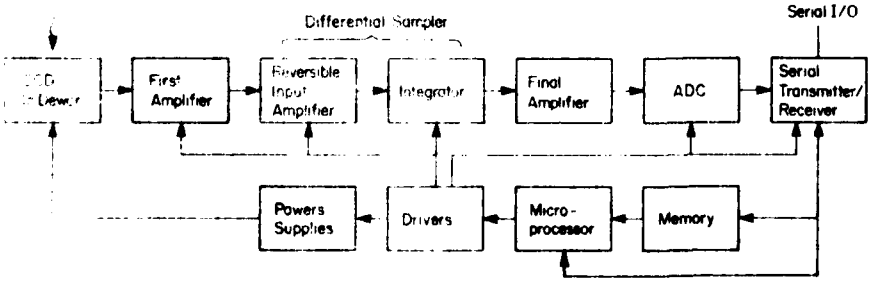

FIG. 4. Block diagram of the CCD electronics.

established in which a 64 × 64 pixel section of the CCD surrounding a star or a spectral line is displayed and optional cuts through the image in the horizontal and vertical directions with corresponding FWHM's may also be displayed. The 64 × 64-pixel region is also used for speckle interferometry.

A cursor can be displayed on the video monitor to mark objects to be photometered, pixel values to be read out, and regions to be averaged. Some simple picture processing routines are available so that subtle features in images may be studied while still at the observatory to see if additional exposures are necessary. Routines are available to perform flat-fielding, dark current and bias subtraction, and to co-add images. Fully automatic operation is possible for which the user is not required to be present; this is useful for taking bias frames and dark frames.

III. THE CCD DEWAR

The liquid nitrogen Dewar for the CCD is a cylindrical chamber 7.75-in. in diam. and 8.5-in. in length with a 9-in. diam. faceplate (see Fig. 2). It is designed to work in an upward- or downward-looking position by interchanging only the external fill and vent tube connections. The CCD socket is screwed to a copper block and the CCD chip is held in place with two copper fingers. The copper block is attached by means of stainless steel standoffs to a 1-liter welded stainless steel liquid-nitrogen bottle. The nitrogen bottle is supported by a combination of Kel-F standoffs and by the 0.5 in. diam 20-mil stainless steel fill/vent tube. Three additional Kel-F rods connect the cylindrical radiation shield to the outer Dewar wall. Flexure is undetectable in this arrangement, and the nitrogen holding time is not seriously degraded by our rigid structure; one filling lasts for 10.5 hr. A photograph of the top of the opened Dewar is shown in Fig. 3.

IV. THE CCD ELECTRONICS AND LOGIC

Figure 4 shows a block diagram of the CCD electronics. The digital signal-processing circuitry is enclosed in a heavily shielded and temperature-controlled chassis divided into separate sections and connected to the Dewar by a triply shielded 18-in.-long cable. Power supplies are mounted outside the box and power is brought in through filtering feedthroughs. Although we initially placed a preamplifier inside the Dewar, we found that greater stability could be achieved without it and at no increase in readout noise. Our output bias level is presently stable to ± 10 electrons over a night.

In the following paragraphs, we discuss the preparation and readout of the CCD and trace the signal through the electronic circuitry. In order to prepare the system for an exposure and readout, the NOVA downloads a variety of subroutines in machine code into the microprocessor memory. The first microprocessor memory location is reserved for a jump instruction which moves the program pointer to the desired program. When the Nova initiates a particular command, it only loads the address of the chosen program into the first microprocessor memory location and starts the microprocessor. An exposure and its preparation consist of the execution of FORTH commands on the NOVA and microprocessor programs which (i) rapidly read out the CCD six times, after which all residual charge from a previous exposure is flushed from the system, (ii) apply the correct voltages for an integration of the CCD electrodes, and finally, (iii) open the shutter for a predetermined period of time. Immediately upon completion of an exposure, a different jump instruction is sent to the CCD and it is clocked in its normal slow-readout mode.

We turn now to the details of shifting the charge on a pixel across the CCD substrate to the output amplifier by stepping voltages on the horizontal and vertical electrodes, and to the sampling and digitization of the charge. The charge on a pixel is most accurately determined by performing a differential sample of the voltage of the on-chip CCD capacitor before and after charge is transferred to it. In our system, we use an up-down integrator for this task.

We shall outline the essential steps in the differential sample, referring the reader to Figs. 5–7 for more specific details of the waveforms. (Our differential sampler is based on a design by Marcus *et al.* 1979). First, the CCD capacitor is reset to a reference voltage, and that voltage is sampled by up-integrating, when switch #2 (integrator) is turned on. Then the integrator is turned off and signal charge is transferred to the CCD capacitor by driving the three horizontal electrodes through a cycle. To perform the down-integration, switch #1 is reversed, and the integrator is turned on again. After the end of the down-integration, the voltage on the integrator is digitized to 14 bits and the integrator reset with switch #3 in preparation for the next cycle. After 320 horizontal advances, charge is shifted by one row in the vertical direction loading the horizontal register, and another 320 horizontal shifts are performed.

As may be seen in Fig. 7, we use three distinct voltage levels on the verticals, in contrast to other groups that use only two voltage levels. The intermediate state is used on all vertical electrodes during the exposure and on vertical electrode #2 during the horizontal transfer. We found that the presence of an intermediate state increases the charge-transfer efficiency and the depth of the potential wells.

Including the timing variables shown in Fig. 8 which show the 8 τ's for the fast reads used for reading the area surrounding a 64 × 64-pixel area, there are a total of 29 timing values. These values are software variables and, consequently, are easily changed. There are nine independent electrode voltages which are set using hardware.

Trimming the differential sampler makes use of both hardware and software adjustments. The product of gain × time must be the same for both the up- and down-integrations during sampling. Three potentiometers (not shown) in the output arms of the switches in Fig. 5 can be adjusted to balance the gain. Final adjustment is most conveniently made by fine-tuning the ratio of the time spent in the up and down portions of the integration. For example, our time interval for up-integration τ_1 is 124.7 μs and the time interval

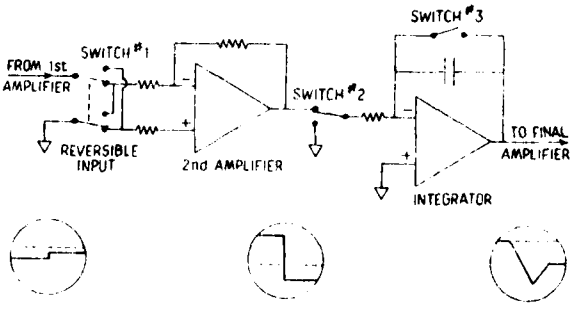

FIG. 5. Schematic diagram of the differential sampler. In the depiction of the waveform at each stage, the dashed line represents zero volts.

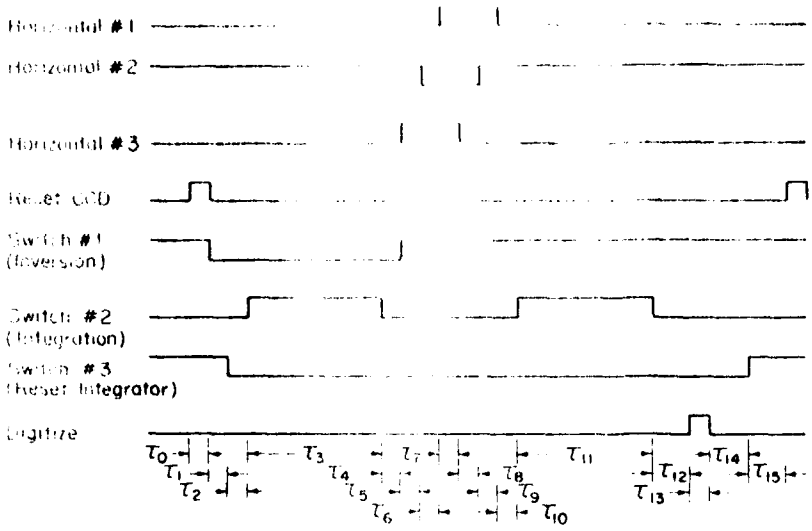

FIG. 6. Timing logic for horizontal transfer and switching.

for double-integration τ_{11} is 125.0 μs. Other timings are discussed in detail in Sec. V, on optimization. With the system balanced, the noise due to the electronics is about five electrons. Compared to the readout noise of 63.9 electrons, the noise due to the electronics makes a negligible contribution to the overall noise since these components add in quadrature.

Because differential sampling is not widely understood, we wish to emphasize the importance of keeping the ratio of integration time to transfer time large when $1/f$ noise is significant, as is the case with CCD on-chip amplifiers. While the contribution to $1/f$ noise is independent of integration time if one neglects the transfer time, a nonzero transfer time results in a signal-to-noise ratio (SNR) proportional to $(1-x)^2$, where x is the ratio of transfer time to total integration plus transfer time (Loh 1977; Hegyi and Burrows 1980). Our horizontal transfer time is 3.4 μs; hence, the SNR is degraded by 2.7% compared to an infinitesimally small transfer time. If the transfer time is 12 μs and the integration time 18 μs for each portion of the differential sample, as in some systems, the degradation is about 44%. It is interesting to compare the SNR obtained with the differential sampling function which we use for our CCD with that of a sampling function optimized for a combination of $1/f$ and white noise (Hegyi and Burrows 1980; Hegyi and Burrows 1984). For small signals, an optimal sampling function could improve the SNR by ~40%. To derive this result, we have estimated that the white-noise power is equal to the $1/f$ noise power at about 100 KHz.

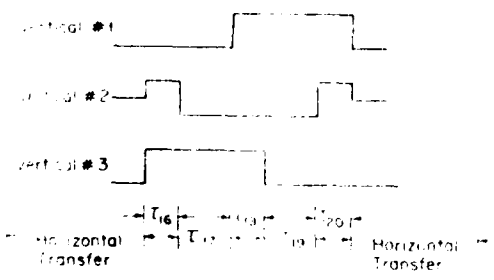

FIG. 7. Timing logic for vertical transfer.

Two problems we did not anticipate during the initial design of the CCD electronics which deserve mention are the generation of light in the on-chip amplifier under certain operating voltages and the drainage of charge during long exposures from several rows of the CCD along the horizontal register. We have since heard that the latter problem has been observed by others. Our solution to both these problems has been to disconnect the on-chip amplifier output and keep the phase reset voltage low during an exposure. A large load resistance for the CCD is only a partial solution to these problems because although it modestly increases the Johnson noise at the input of the first amplifier, it, more importantly, decreases the signal power received from the CCD relative to the background-noise power. A lower CCD temperature also decreases the charge leakage, but the temperature is constrained by factors discussed in Sec. V. By disconnecting the amplifier output we are able to use a moderately low resistance in the source follower, 2000 Ω.

V. OPTIMIZATION OF CCD PERFORMANCE

We spent considerable time and effort optimizing the performance of our CCD. Our CCD exposures are now characterized by excellent resolution, large dynamic range, and an imaging area essentially free of blemishes. The desired characteristics for the performance of a CCD system are summarized in Table I. To achieve this, the parameters in our system listed in Table II were designed to be adjustable.

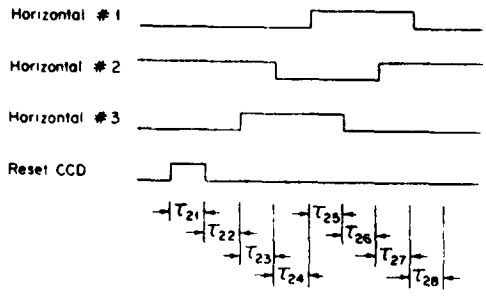

FIG. 8. Timing logic for fast readout.

TABLE I. Desired characteristics of a CCD system.

A	The CCD
	1. Large dynamic range (low readout noise and deep potential wells)
	2. High resolution
	3. Small number of blemishes
	4. No leakage of charge from wells
	5. Low dark current
	6. Low noise pickup
	7. Time stability
B	The Electronics
	1. Lowest possible noise
	2. No saturation
	3. Perfect differential sampler
	4. Time stability

TABLE II. Available control parameters.

A.	Voltages
	1. 6 Horizontal (2 states for each of 3 electrodes)
	2. 9 Vertical (3 states for each of 3 electrodes)
	3. Reset drain, output drain, and phase reset
B.	Timing Values—29 Total
C.	Timing and Switching Logic
D.	Temperatures of CCD Chip and Electronics

After the system was constructed, we first adjusted the parameters to obtain a usable picture from the CCD. Next, we began a long series of tests to fine-tune the system. The process of optimization is complicated by the fact that a single control parameter can affect more than one CCD characteristic and, consequently, adjusting one control parameter may necessitate readjusting another. These interactions, however, are not serious, and in most cases the CCD's characteristics are unchanged by a small variation in the value of a parameter.

A large dynamic range is achieved by optimizing the CCD so that the potential wells can be filled to their maximum capacity. With a readout noise of about 64 electrons for the RCA thinned chip, a dynamic range of about 5500 can be attained. Whereas the readout noise is mostly determined by the $1/f$ noise spectrum of the on-chip amplifier and is sensitive to timing ratios in the differential sampling function, the ability of the potential wells to hold charge is strongly determined by the voltages on the horizontal and vertical transfer electrodes.

In order to determine a first approximation to the operating potentials of the electrodes and so obtain a usable picture, we exposed the CCD to light of an intensity and duration such that the wells would be filled to their maximum level. The empirically determined voltage ranges to prevent bleeding of charge are given in Table III. The voltage limits were less stringent at lower exposure levels; hence, adjustment at a high exposure level guarantees a large dynamic range.

Having determined a range of electrode potentials which gave the largest dynamic range, the next step was to determine the potentials which gave the best resolution. Because the resolution is adversely affected by the number of transfers of a charge packet before it is deposited onto the on-chip capacitor of the CCD and by low light levels (the threshold effect), we achieved the greatest sensitivity for improvement of resolution by imaging a faint point-like source (a pinhole in aluminum foil whose image was larger than one pixel) onto the last area of the CCD to be read out. The resolution was most sensitive to the potential on horizontal electrode #3. By making the voltage swing during transfer larger on this electrode than on those of the other horizontal electrodes, i.e., -7 to $+6$ V compared to -5 to $+5$ V, the resolution was noticeably improved. The potential on horizontal electrode #2 had less of an effect, but when the voltage swing was set to only -4.5 to $+4.5$ V, defects appeared on the screen and the resolution deteriorated.

The resolution is also strongly affected by the time spent transferring charge. In general, a longer transfer time gives higher resolution, but at the expense of increased blemishes. In addition, the vertical timing values and the vertical electrode potentials are weakly coupled. Referring to the timing logic diagram in Fig. 6, we found that the horizontal transfer times τ_5, τ_6, and τ_9 had little or no effect upon either the resolution or the blemishes. Making τ_7 longer (up to 1.2 μs) improved the resolution; however, pulse feedthrough on the chip increased the readout noise. A good compromise for τ_7 was 0.5 μs. Making τ_8 longer also improved the resolution, but at the expense of increased blemishes. Its value was set to 0.3 μs.

For the vertical transfer times (see Fig. 7), increasing τ_{16} and τ_{18} improved the resolution slightly, but also increased the number of vertically oriented blemishes. Increasing τ_{17} and τ_{19} improved the resolution, but also increased the number of blemishes, though τ_{20} had no effect on resolution and blemishes. By making the high state voltage on vertical electrode #3 more negative, the number of blemishes could be reduced, but at the expense of reduced well capacity (observed as bleeding of the image at high exposure levels). The voltage levels at which the number of blemishes were reduced and at which bleeding appeared were found to be affected by the vertical transfer times. The best compromise for electrode potentials is listed in Table IV. The effect of temperature on resolution is discussed at the end of this section.

When the CCD is operated in its focusing mode, a 64×64-pixel area is read out with the same electrode voltages and timing values as for the full frame, but the surrounding pixels are read out at a much faster rate. The time intervals τ_{21} through τ_{28} control this fast readout and the timing logic is

TABLE III. Electrode potentials for which bleeding of charge did not occur.

Electrode number	High state	Low state	Intermediate state
Horizontal 1	$3.5 < V < 6.5$	$-5.9 < V < -1.7$	
Horizontal 2	$-3.0 < V$	$V < -3.0$	
Horizontal 3	$1.7 < V$	$-7.9 < V < -3.4$	
Vertical 1	$-0.8 < V$	$V < -8.0$	$V < -2.4$
Vertical 2	$V < -2.0$	$V < -8.0$	$-4.0 < V < 0.0$
Vertical 3	$-0.6 < V$	$V < -8.0$	$V < -1.0$

Note to TABLE III

Only the vertical electrodes have an intermediate state.

TABLE IV. Best CCD voltages.

Electrode number	High state	Low state	Intermediate state
Horizontal 1	5.0	5.0	
Horizontal 2	5.0	5.1	
Horizontal 3	6.0	7.0	
Vertical 1	0.5	9.4	9.0
Vertical 2	−4.0	9.4	2.0
Vertical 3	−1.5	9.4	9.0

RD 12.8
OD 10.8
ϕ_R 8 and −8

shown in Fig. 8. We found that the readout noise is slightly dependent on τ_{22} and τ_{28} and that values of 4.2 μs give about a 4% reduction in noise compared to 0.3 μs.

We also operate the CCD in a mode called "speckle" which is designed for short exposures of the highest possible resolution. This mode is similar to the focus mode described above, except that the 64×64-pixel area is placed in the upper left of the CCD frame (the first area to be read out), and hence undergoes the smallest number of transfers before being sampled. In this mode, 32 consecutive frames are recorded on tape. We were able to increase τ_5 through τ_9 so that the total horizontal transfer time was 6 μs and to increase τ_{16} through τ_{20} to 1.2 μs without producing blemishes. The improvement in resolution was 27% as determined by measuring the FWHM of a point-like light source imaged onto the CCD. For our full-frame format and the long exposures required by astronomical objects, the resolution is as good as in the speckle mode; this is because the longer exposure times allow a sky background to build up which eliminates the threshold effect.

The threshold effect, which is eliminated with a background of about 300 electrons, was investigated by imaging faint point-like images on an adjustable background. In the upper left corner, however, there is no measurable threshold effect. The fast read τ's, τ_{24}, τ_{25}, and τ_{26} were, in addition, increased to 1.2, 0.7, and 0.6 μs in order to improve the uniformity of the bias exposure (zero incident light, zero exposure time).

Several schemes for the timing and switching logic were tried. Our first arrangement (based on the RCA data sheets) used four fewer time intervals for the horizontal transfer. A shorter total time for transfer was expected to give lower readout noise, as explained in Sec. IV. With this switching logic, the electrodes have different potentials before and after charge transfer and, because of feedthrough effects in the CCD, an offset voltage developed which caused saturation in the amplifier chain. Because the time between integrations is constrained by its effect on resolution and blemishes, the $1/f$ noise and the white noise can be made smaller by lengthening the integration times (the integration times, τ_1 and τ_{11}, also control the gain of the amplifier chain). Other optimizations of the timing included determining the best values to avoid feedthrough and pickup of timing signals by the integrator. In particular, τ_1, τ_2, and τ_{10} should be slightly greater than 1.2 μs. The best values for the timings are listed in Table V.

We found that the chip temperature, in addition to affecting the loss of charge near the horizontal register mentioned in Sec. IV, also controls the quantum efficiency and the resolution. For each degree drop in temperature, the quantum efficiency decreases by about 0.3% (tested at a wavelength of 5500 Å and between 107 and 173 K). The resolution was found to be best at 152 K, with the FWHM of a point-like image being 41% larger at 10 deg higher or lower than the optimal temperature (see Fig. 9). Note that the minimum FWHM in Fig. 9 is constrained by the size of the point-like image we used. Although we can obtain a FWHM of unity, e.g., on spectral emission lines, the actual value depends on the placement of the image relative to a pixel's boundary. Here we avoided that problem by using a larger image. We estimate the accuracy of our temperature measurements to be approximately three degrees.

TABLE V. Timing values.

Tau	Time (μs)
0	0.3
1	1.5
2	1.6
3	124.7
4	0.3
5	0.3
6	0.3
7	0.5
8	0.3
9	0.3
10	1.4
11	125.0
12	0.6
13	0.3
14	13.0
15	28.6
16	0.5
17	1.0
18	0.5
19	1.0
20	0.7
21	0.3
22	4.2
23	0.3
24	0.3
25	0.5
26	0.3
27	0.3
28	4.2

Precise control of the CCD temperature is important not only for assuring that one is always within the optimum range of operation, but also to stabilize the bias level at the input of the amplifier chain. For each degree change in temperature of the CCD, the input bias (equal to the voltage drop across the CCD load resistor) changes by 3.1 mV. As we mentioned in Sec. IV, the output bias level is made relatively insensitive to this change by carefully balancing the differential sampler by adjusting τ_3. We stabilize the tem-

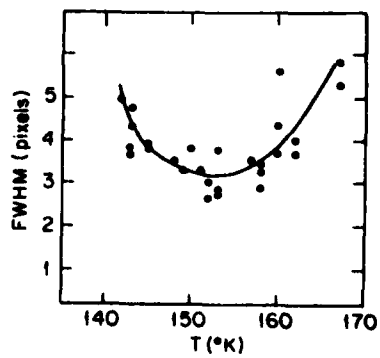

FIG. 9. Dependence of resolution on CCD temperature.

perature of the CCD by a very high-gain feedback loop which drives a heating element, two resistors mounted inside a copper block onto which the CCD is attached. Operation at an average power input of about 1 W gives some additional sensitivity (depending on the square root of the power) and does not seriously decrease the holding time for liquid nitrogen in our Dewar.

VI. DETERMINATION OF CCD NOISE

The readout and spatial noise of a CCD are of importance because the former determines the minimum detectable signal for situations with a small number of collected photons per pixel such as spectroscopy and speckle interferometry, while the latter sets the limit for a large number of collected photons such as the detection of faint features superimposed on a night-sky background. Although spatial noise can be corrected by dividing by a flat-field exposure, the variation in quantum efficiency with wavelength from pixel to pixel is sufficiently large that differences between the spectrum of the signal and that of the flat field become important at roughly the level of a few parts in 1000, for wavelengths near bright night-sky lines.

The measurement of readout noise can be done in two ways. The methods start from the basic equation

$$\sigma_{t,e}^2 = \sigma_{r,e}^2 + \sigma_e^2 + \sigma_{s,e}^2, \tag{1}$$

where $\sigma_{t,e}$ is the total noise, $\sigma_{r,e}$ the readout noise, σ_e the shot noise, and $\sigma_{s,e}$ the spatial noise. All quantities are on a per pixel basis and are measured in units of electrons. If we define the gain g as ADU/n_e, where ADU represents observed analog-to-digital units and n_e is the corresponding number of electrons, and define F_s, the fractional spatial noise, as $\sigma_{s,e}/n_e$, then because $\sigma_e = \sqrt{n_e}$ we find the total noise in ADU to be

$$\sigma_{t,\mathrm{ADU}}^2 = \sigma_{r,\mathrm{ADU}}^2 + g\cdot\mathrm{ADU} + F_s^2\mathrm{ADU}^2. \tag{2}$$

The first method makes use of a least-squares fit of the observed $\sigma_{t,\mathrm{ADU}}^2$ versus ADU data to the above second-order equation. It is not difficult to show that each point must be weighted by

$$\frac{(n_p - 1)n_0}{2\langle\sigma_{t,\mathrm{ADU}}^2\rangle^2}, \tag{3}$$

where n_p is the number of pixels in each exposure and n_0 is the number of repeated observations of each point. If information about the spatial noise is not needed, some computation can be saved by fitting to a first-order equation after removing the spatial noise from the data. There is an advantage to this second method in that any nonlinearities become readily apparent. The spatial noise is removed by averaging many exposures and computing the mean error about the mean value in ADU for each pixel. A variation of the second method and our chosen approach removes the spatial noise by taking only two exposures. It can be shown that the best estimator of the total noise minus the spatial noise, $\sigma_{t-s,\mathrm{ADU}}^2$, is

$$\sigma_{t-s,\mathrm{ADU}}^2 = \frac{\sum_i (\mathrm{ADU}_1 - \mathrm{ADU}_2)_i^2}{2n_p}, \tag{4}$$

where the sum is over all pixels n_p in the area. We expose twice on an area of 50×50 pixels. A sample plot from which the gain and readout noise can be obtained is given in Fig. 10.

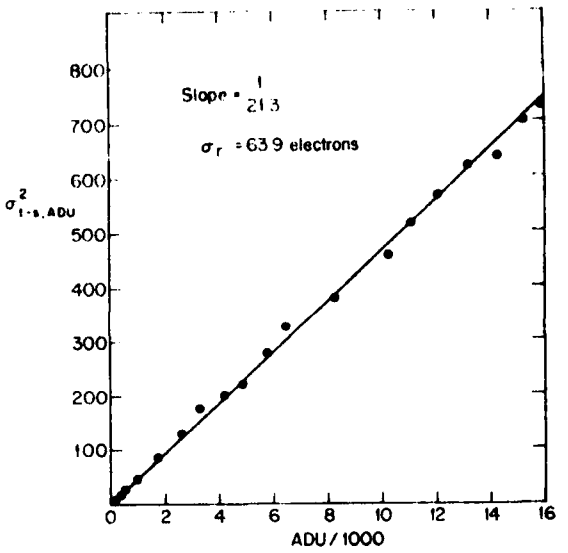

FIG. 10. Determination of CCD gain and readout noise. $\sigma_{t-s,\mathrm{ADU}}$ is the total noise less the spatial noise measured in ADU.

In this case, the reciprocal of the gain $1/g$ is 21.3 electrons/ADU and the readout noise is 63.9 electrons.

As a check to verify that we understand the origin of the readout noise, we can calculate the noise using the measured CCD capacitance and the measured $1/f$ noise of the on-chip amplifier. By measuring the current into the CCD through RD, the voltage across the load resistor as the CCD is being read out, and our cycle time, we obtain a value for the on-chip capacitance of 0.62 pF. To determine the noise spectrum we measured the noise of the CCD output MOSFET from 200 to 25 000 Hz with a calibrated noise-spectrum analyzer. Over this range, the noise power spectrum closely follows a $1/f$ law of the form F_0/ν, where F_0 is $230(\mu\mathrm{V})^2$. The measured exponent of ν is 1.12 ± 0.05. Estimating, as in Sec. IV, that the white-noise power equals the $1/f$ noise power at 100 kHz, we calculate (Loh 1977; Hegyi and Burrows 1980) the readout noise to be 56.7 ± 6 electrons. The error represents an estimate of our overall measuring accuracy. The measured and calculated readout noise are in reasonable agreement.

By measuring the readout noise as a function of pixel location on the CCD, we find that the readout noise is position dependent. Figure 10 shows data taken in the upper-left corner of the chip, but in other locations the shape of the curve is no longer straight. For these areas, the measured total noise at intermediate level exposures (up to 200 000 electrons) is a few percent higher than the shot noise. This is most likely due to the greater contribution of transfer noise and trapping noise, both of which depend on the square root of the total number of transfers (Beynon and Lamb 1980). At higher levels (up to 350 000 electrons, a limit set by our ADC), we observe the same noise at all locations. Also, when no light is incident on the CCD, the noise is essentially the same everywhere.

A measure of the spatial noise as a function of wavelength and sample size was obtained by computing the standard deviation of a square area of a twilight-sky flat-field exposure as a function of the length of an edge of the square after removing the contribution due to readout and shot noise.

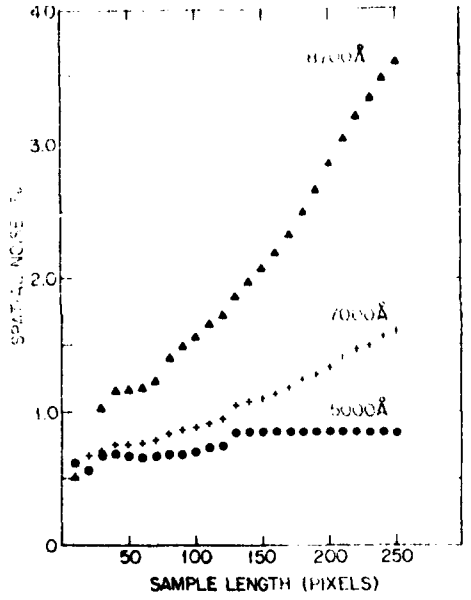

FIG. 11. CCD spatial noise as a function of wavelength and sample size.

From the plot of this data shown in Fig. 11, we see that the corrections for spatial noise become increasingly important at longer wavelengths and larger pixel sample sizes. Flat-field exposures taken of the dawn and twilight skies on different nights are consistent with each other on the large scale (the upper third compared with the lower third of the frame) from one part in 100 000 to a few parts in 10 000 peak to peak.

A complete correction of an exposure for spatial noise and zero level is carried out on a pixel-by-pixel basis using the expression

$$\frac{[(\text{exposure} - \text{bias}_E) - (\text{dark frame} - \text{bias}_D)]\text{scale}}{(\text{flat-field} - \text{bias}_F)}, \quad (5)$$

where the dark frames and flat fields are averages of many exposures and the scale is a normalization constant which could be set equal to the average intensity of a pixel for the average of the flat-field exposures. Each processed exposure must have a constant bias value for the exposure, dark frame, and flat field (bias_E, bias_E, and bias_F, respectively) subtracted; in our system, these are computed from an average of a 50×50-pixel area which is read out immediately following readout of the full frame. Dark frames for exposure times from zero to more than 45 min show structure on the large scale of about 40 electrons peak to peak. Because this can be as much as 1% of the sky level, it is important to subtract this structure from an exposure. At our operating temperature, the dark current contributes about 25 electrons per hour per pixel on average, with small pixel-to-pixel variations.

CCD's are quite sensitive to background low-frequency electromagnetic radiation. We found that a small ripple voltage on the shutter power supply filled pixels with charge at a rate several hundred times larger than the normal dark current. After eliminating the ripple so that the shutter voltage was purely dc, even under load, this problem disappeared.

VII. PICTURE PROCESSING

Our picture processing is done on a VAX/780 computer running under VMS. Images are displayed on a Grinnell GMR270. The Grinnell with joystick-controlled quad cursors and zoom and pan enable us to display images in 4096 pseudocolors. Two VT100 terminals with graphics, a Printronix, a Tektronix 4662 flat-bed plotter, and the Grinnel are each capable of displaying plots.

We have written most of our present software for the reduction of two-dimensional surface photometry of galaxies. The most notable subset of these routines can do a weighted least-squares fit of any chosen surface-brightness formula to an elliptical galaxy's light distribution, while taking into account overlapping stars and galaxies, including seeing effects, yielding the fitting parameters of the formula with their errors. We are currently writing programs to handle two-dimensional spectra. Some programs which were written at Mount Stromlo Observatory, Australia by Greg Quinn, Reet Valek, and Dennis Warne do fast data transfer to and from disk in a format called Standard Astronomical Data (SAD). A 320×512 array of REAL*4 data can be transfered in about 5 s. Copies of the Mount Stromlo programs were transmitted to us by Susan Simpkin. We have given the acronym MIIPS (Michigan Image Processing System) to our picture-processing software.

An example of the quality of our CCD images is shown in Fig. 12. It is a 30-min exposure of the field surrounding NGC 4874 in the Coma cluster taken through a 1000-Å bandpass filter centered at 5000 Å. This exposure, for which the entire frame is shown, has not been flat-fielded or edited in any way, yet there is no evidence of fringing or of charge trailing due to imperfect charge-transfer efficiency. There is one minor blemish in two adjacent columns extending over 34 rows. Although the bright star has saturated the ADC (more than about 350 000 electrons/pixel) in 43 pixels, the star image appears unbroadened with no bleeding of charge, and even diffraction spikes are visible.

In other exposures, we have found fringing at less than 2% of the sky level in the I band, centered at 8700 Å, but at 5500 Å, only one exposure out of 50 has shown fringing. It was observed to be at a level of less than 1% of the sky level.

We have tested the linearity of the system in three ways. By exposing on a constant uniform source of light and then plotting the observed signal in ADU against exposure time, we see no departure from linearity from our shortest exposures (less than 10 ms) to the highest level our ADC can record (16 383 ADU or 348 958 electrons). By measuring the total light in the images of calibration stars observed at a variety of exposure times and for a variety of magnitudes, we obtain a calibration curve with a standard deviation for a single observation of 0.0075 (0.75%). It is interesting to note that we can calibrate on stars as bright as Vega. The exposure times must be kept below 1 s and the images defocused.

A more stringent test of linearity is defined on the scale of a pixel. That is, if at high levels of illumination, charge drains to neighboring pixels but the total charge is conserved, the above two tests will indicate linearity although it is violated on a per pixel basis. By measuring the FWHM of point-like images as the illumination was increased from very low levels up to saturation of our ADC, we observed no increase in the FWHM of the image.

As an example of image processing with our system, Fig. 13 shows the processed field of Fig. 12 with the brightest galaxy modeled by our programs and subtracted from the

FIG. 12. Thirty minute CCD exposure of NGC 4874 (Coma cluster) at 5000 Å. No flat-fielding has been done.

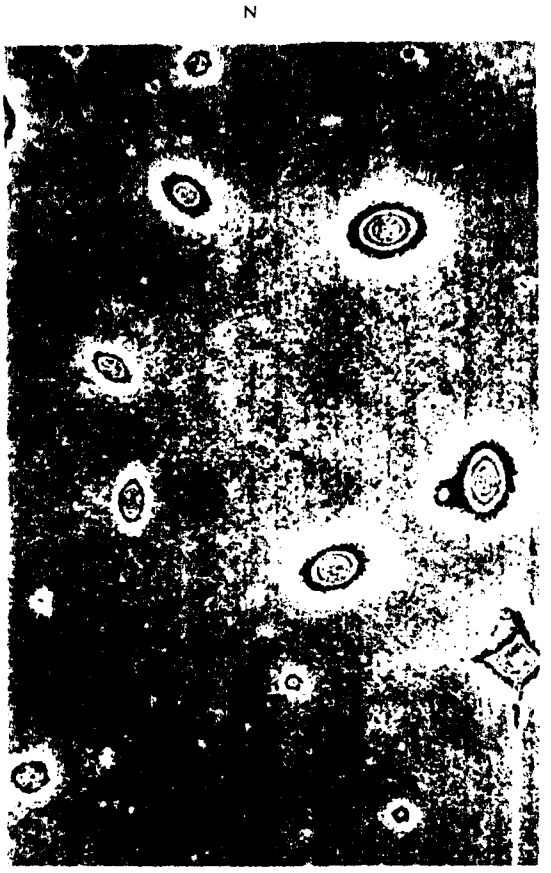

FIG. 13. Same as Fig. 11, but with NGC 4874 modeled and subtracted.

frame. The contrast of the Grinnel was increased slightly for Fig. 13 as compared to Fig. 12. For this figure, we use a logarithmic look-up table which equates a 1% change in intensity with the smallest visible change in grayscale level. Except for the central three pixels, the mean surface brightness of a circular contour has a maximum deviation from the sky level of only one part in 2300 when compared to the central surface brightness of NGC 4874. This deviation is typical of a blank region of sky. The faintest objects visible in Fig. 13 are about 23^{m}.6 (based on $m_{5000} = 0.0$ for Vega). A similar modeling and subtraction for an exposure of M87 reveals globular clusters to the very center of the galaxy.

We would like to acknowledge the help of students Tim Frank, John Haggis, Jim Haywood, Stephen Russell, Slava Sharkin, and Doran Smith, and the support of Air Force Grant No. AFOSR-80-0095.

REFERENCES

Archer, G. F., Fompsett, M. F., and Smith, G. E. (1970). Bell Syst. Tech. J. **49**, 593.

Beynon, J. D. E., and Lamb, D. R., editors (1980). *Charge Coupled Devices and Their Applications* (McGraw Hill, London and New York).

Dewey, D., and Ricker, G. R. (1980). In *Proceedings of the SPIE Conference on Applications of Digital Image Processing to Astronomy, Pasadena, Cal.*, edited by D. Elliott (The International Society for Optical Engineering, Bellingham, Wash.), Vol. 264, pgs. 42–47.

Hegyi, D. J., and Burrows, A. (1980). Astron. J. **85**, 1421.

Hegyi, D. J., and Burrows, A. (1984). Astron. J. **89**, 1629(E).

Kaitchuck, R. W., Schild, R. E., Gursky, H., Madejski, G. M., Schwartz, D. A., and Weekes, T. C. (1980). Publ. Astron. Soc. Pac. **92**, 733.

Kreidl, E. D. (1977). Ph.D. thesis, Princeton University.

Kreidl, E. D. (1981). In *Proceedings of the SPIE Conference on Solid State Imagers for Astronomy, Cambridge, Mass.*, edited by J. C. Geary and D. W. Latham (The International Society for Optical Engineering, Bellingham, Wash.), Vol. 290, pgs. 150–154.

Marcus, S., Nelson, R., and Lynds, R. (1979). In *Proceedings of the SPIE Conference on Instrumentation in Astronomy III, Tuscon, Ariz.*, edited by D. L. Crawford (The International Society for Optical Engineering, Bellingham, Wash.), Vol. 172, pgs. 207–231.

Meyer, S. S., and Ricker, G. R. (1980). In *Proceedings of the SPIE Conference on Applications of Digital Image Processing to Astronomy, Pasadena, Cal.*, edited by D. Elliott (The International Society for Optical Engineering, Bellingham, Wash.), Vol. 264, pgs. 38–41.

Robinson, L. B. (1981). In *Proceedings of the SPIE Conference on Solid State Imagers for Astronomy, Cambridge, Mass.*, edited by J. C. Geary and D. W. Latham (The International Society for Optical Engineering, Bellingham, Wash.), Vol. 290, pgs. 124–129.

Wright, J. F., and Mackay, C. D. (1981). In *Proceedings of the SPIE Conference on Solid State Imagers for Astronomy, Cambridge, Mass.*, edited by J. C. Geary and D. W. Latham (The International Society for Optical Engineering, Bellingham, Wash.), Vol. 290, pgs. 160–164.

END

FILMED

10-85

DTIC